Astron. Astrophys. 292, 381–391(1994)

ASTRONOMY AND ASTROPHYSICS

A search for dark matter in elliptical galaxies: radially extended spectroscopic observations for six objects*

G. Bertin[1], F. Bertola[2], L.M. Buson[3], I.J. Danziger[4], H. Dejonghe[5], E.M. Sadler[6], R.P. Saglia[7,8,11], P.T. de Zeeuw[9], and W.W. Zeilinger[10,12]

[1] Scuola Normale Superiore, Piazza dei Cavalieri, I-56126 Pisa, Italy
[2] Dipartimento di Astronomia, Padova, Italy
[3] Osservatorio Astronomico, Padova, Italy
[4] ESO, Garching bei München, Germany
[5] RUG Observatorium, Gent, Belgium
[6] School of Physics, University of Sydney, Australia
[7] Landessternwarte, Heidelberg, Germany
[8] Dipartimento di Matematica, Pisa, Italy
[9] Sterrewacht Leiden, The Netherlands
[10] ST–ECF, Garching bei München, Germany
[11] Present address: Universitäts-Sternwarte München, Germany
[12] Present address: Institut für Astronomie, Wien, Austria

Received 21 March 1994 / Accepted 17 May 1994

Abstract. Within the ESO Key Programme "A search for dark matter in elliptical galaxies", we have performed a detailed study of the large scale stellar kinematics of NGC 1400, 4946, 5812, 6721, 7507, and 7796. Our observations have produced kinematical data down to the 24.1 mag arcsec^{-2} in the B band, i.e. in some cases out to 2 R_e and beyond. NGC 1400, 4946, and 6721 show significant rotation. The other three galaxies (NGC 5812, 7507, and 7796) can be described by spherical non-rotating equilibrium models. For two of these objects self-consistent stellar dynamical models with constant mass-to-light ratio are found to give good fits to the photometric and kinematical data, although the presence of dark matter is not excluded. In contrast, NGC 7796 shows evidence for the presence of a dark halo. This galaxy also exhibits counterrotation inside 4″ and, correspondingly, a central peak in the velocity dispersion profile. On the basis of the small sample of objects studied so far, with radially extended spectroscopic observations, possible trends in the size of dark halos around elliptical galaxies are pointed out.

Key words: galaxies: elliptical, NGC 7796, kinematics and dynamics – dark matter

1. Introduction

The study of spiral galaxies has given convincing evidence for the presence of dark halos. The evidence comes primarily from the kinematics of smooth, symmetric H I disks that extend much further out than the stellar optical disks. Optical data alone neither require nor rule out the presence of dark halos (Kalnajs 1983; Kent 1986). The conservative effort to minimize the role of invisible matter leads to the so-called maximum disk solutions (van Albada & Sancisi 1986). These may overestimate the actual M/L ratio for the disk, as is especially clear from the modeling of the Milky Way Galaxy (Kuijken & Gilmore 1989; Merrifield 1992). Whatever the specific modeling choices may be, unless one is willing to modify the laws of gravity (Milgrom 1983), it is generally agreed that dark matter exists in spiral galaxies in the form of diffuse halos.

For elliptical galaxies the situation is less clear (Sarazin 1987; Sancisi & van Albada 1987; see also the more recent reviews by Kent 1990 and Ashman 1992), but it may be explored in the light of what has been learned from the study of spiral galaxies. The aim of the ESO Key Programme "A search for dark matter in elliptical galaxies" (Bertin et al. 1989) was to clarify the properties of the mass distribution in elliptical galaxies by (i) investigating the velocity field of the gaseous component for those ellipticals which possess a disk of ionized gas and by (ii) measuring stellar velocity dispersion profiles out to large radii. In the first part of the ESO Key Programme, which will be reported separately, the kinematics of the ionized gas is modeled assuming that the gas occupies closed non-circular orbits in a

Send offprint requests to: G. Bertin

* Based on observations collected at the European Southern Observatory, La Silla, Chile

Table 1. Properties of the programme galaxies

Object	Type[1]	D[2] (Mpc)	$m_B^{(2)}$	$R_e^{(2)}$ ($''$)	$\mu_B[R_e]$[3] (mag arcsec^{-2})	Phot. source
NGC 1400	SA0$^-$	40	11.62	38$''$	22.28	(4)
NGC 4946	E$^+$?	58	12.92	17$''$	22.88	(3)
NGC 5812	E0	42	11.90	24$''$	22.24[5]	(5)
NGC 6721	E$^+$:	88	12.73	23$''$	22.42	(3)
NGC 7507	E0	35	11.15	31$''$	22.32	(4)
NGC 7796	E$^+$	65[6]	12.28	27$''$	22.65	(4)

References: (1) RC3, de Vaucouleurs et al. (1991). (2) From Faber et al. 1989 (H_0 = 50). (3) Lauberts and Valentijn (1989). (4) Bender, unpublished data. (5) From Djorgovski (1985), converted from R band using $B - R = 1.7$. (6) From redshift of Faber et al. 1989 (H_0 = 50).

Table 2. Observing log

Date	Object	P.A.	Effective slit scale (arcsec pixel^{-1})	Exp. time (hours)	Total exp. time (hours)
May 9–11, 1989	NGC 4946	143°	0.89	2	
		143°	4.45	2+2+2+2	10
	NGC 5812	328°	0.89	2	
		328°	4.45	1.5+2+2	7.5
	NGC 6721	331°	0.89	2	
		331°	4.45	1+1+1.5+2	7.5
Nov. 1–5, 1989	NGC 1400	39°	4.45	2.3+2.5+2.8+3+3	13.4
	NGC 7507	285°	4.45	3+3+3+3	12.0
	NGC 7796	348°	1.78	2.2	
		348°	4.45	1.6+2+2	7.8

triaxial potential. This constrains the shape and the mass distribution of the host galaxy, thus providing the mass–to–light ratio M/L as a function of radius. Imaging observations for this part of the project have been presented recently (Buson et al. 1993).

In this paper we report on the second part of the ESO Key Programme. While the photometric profiles of elliptical galaxies are well described by one universal law (the $R^{1/4}$ law, de Vaucouleurs 1948, 1953), their velocity dispersion profiles display a wide range of shapes (Illingworth 1983). This kinematic diversity may be interpreted as evidence for the presence of various amounts of dark matter or of different, and sometimes peculiar, distributions of stellar orbits (Tonry 1983). Our plan is to clarify the role of dark matter in ellipticals by obtaining accurate and radially extended kinematical profiles, i.e. by improving the observational input, and by applying newly developed modeling techniques that complement each other. On the one hand, we can test the viability of the physical picture that, from the dynamical point of view, elliptical galaxies are the result of incomplete violent relaxation (van Albada 1982), with a pressure tensor that is quasi-isotropic in the inner regions and gradually radially biased outside R_e; a fitting procedure has been developed in this context which can identify the amount and distribution of dark matter present (Bertin et al. 1992, hereafter BSS; Saglia et al. 1992, hereafter SBS). On the other hand, using a quadratic programming technique (Dejonghe 1989), we can derive a best-fit distribution function for stellar orbits that would be required by the available photometric and kinematical data under the assumption that dark matter is either absent or distributed as the luminous matter (i.e., that the mass-to-light ratio is constant). To be sure, both modeling procedures assume spherical symmetry and insignificant rotation; for those objects where we may find evidence against these assumptions, the results of the models should be taken with caution.

With this aim in mind, we have carried out deep spectroscopic observations for six apparently round ellipticals of the Southern Hemisphere. In the following section we summarize these observations and the data reduction. Then in Sect. 3 we proceed to illustrate the kinematical profiles derived by application of the Fourier Correlation Quotient method. In Sect. 4 we present the stellar dynamical models. The properties of the line profiles predicted by our best-fit models are also briefly discussed. In Sect. 5 the results obtained in this paper are compared with those obtained from recent observations of three additional objects (Saglia et al. 1993, hereafter SKP), and we discuss some conclusions on the problem of dark matter that can be drawn on the basis of the sample of objects studied so far.

2. Observations and data reduction

Given the goal to measure kinematical profiles as far out as possible relative to the effective radius R_e, a list of candidate ellipticals was selected, based on the following criteria:

(a) A relatively high surface brightness of the galaxy is desired at large radii in order to maximize the signal-to-noise ratio. For the selected objects we have $\mu_B(2R_e) < 24.2$ mag arcsec^{-2}.

(b) A reliable subtraction of the sky background is required for a correct determination of the absorption lines at very faint levels. Given the length of the slit (4′) of the spectrograph available for the observations, this requirement suggests the selection of objects with $R_e \leq 30''$, in order to reach out at a location where the galaxy light is expected to contribute less than 1% of the sky level.

(c) Objects with a large central velocity dispersion are preferred in order to minimize the error bars at the outermost kinematical point relative to the central velocity dispersion (see Sect. 3.3 of SBS);

(d) Round galaxies (E0-E1) are preferred, in order to simplify the theoretical analysis of the results.

The relevant parameters of the six galaxies are given in Table 1. The value of the effective radius R_e , defined as the radius of the aperture that encloses half of the projected luminosity of the galaxy, is a reference value, taken from Faber et al. (1989). RC3 (de Vaucouleurs et al. 1991) reports similar values, except for NGC 1400 (RC3: $R_e = 29''$) and for NGC 7796 (RC3: $R_e = 21''$).

The observations were carried out in two observing runs (May and November 1989) at the ESO/MPI 2.2-m telescope at La Silla, using the Boller & Chivens Cassegrain spectrograph. The detector employed was an RCA SID 006 EX 1024 × 640 pixel CCD with a pixelsize of 15 × 15 μm^2. A 600 grooves mm^{-1} grating was used in second order with a dispersion of 59 Å mm^{-1} in the wavelength region of 4750 – 5670 Å. A slit width of 2.5″ yielded an effective instrumental dispersion of about 60 km s^{-1}. The typical seeing ranged between 1″ and 1.8″ FWHM. The spectral range covered the following absorption lines used in the subsequent analysis: Mg I (λ5175 Å), the E–band (λ5259 Å) and the Fe (λ5270 Å and λ5335 Å) lines.

The 4′ slit of the spectrograph was always aligned with the optical major axis of the galaxy. The center of the galaxy was placed at one extreme of the slit. This allowed a reliable sky determination at a typical distance of about 8 R_e from the galaxy center. The "optimal" exposure time was calculated on the basis of the requirements from the noise sources (Poisson noise, cosmic ray events, and read–out–noise) of the CCD. Given the rather high read–out–noise (55 electrons with a conversion factor of 7.2 electrons/ADU), a substantial increase of the S/N ratio in the outer regions of the galaxy was obtained by binning the pixels of the CCD in the spatial direction and by making the exposure time as long as possible. In most cases, every 5 pixels of the CCD were combined in the spatial direction yielding an effective scale of 4.45″ pixel^{-1}. Some spectra were also obtained without rebinning the CCD so as to use the full spatial resolution provided by the instrument for the central parts of the galaxy. The length of the exposure time was constrained by the frequency of cosmic ray hits on the detector. As a reasonable compromise, the typical integration time of a single exposure ranged between 2 and 3 hours. We estimate that in a typical 3 hrs exposure less than 1% of the pixels are affected by cosmic rays. We took several exposures to increase the signal–to–noise ratio in the outer parts. The total exposure time was typically 8–12 hours per galaxy.

The observing log for the two runs is given in Table 2. Each galaxy spectrum was bracketed by two helium–argon arc spectra in order to check whether shifts along the dispersion occurred, caused by instrumental flexure of the spectrograph during the integration. In the worst case this shift was found to be of 2.26 pixels for a three hours exposure. In addition, in each night a set of spectra of non–rotating G/K–type giant stars was secured with the same instrumental setup, to be used as velocity templates.

The spectra were reduced using the IHAP and MIDAS reduction software at ESO Garching. The data reduction consisted of the standard calibration procedures of bias and dark current subtraction, flat–fielding and correction for distortion. For flat fielding both spectra obtained in the dome with a continuum light source and spectra obtained on an empty sky region at twilight were used. The flat fields were usually able to correct the galaxy spectra to a level of $< 1\%$ accuracy. Examination of the bias overscan region of the CCD revealed that some light from the brightest part of the galaxy is scattered further out. In the case of NGC 7507, which may be considered to be typical for this purpose, the scattered light contribution was found to be about 0.2% of the total signal at a distance of 50″ from the nucleus, with a decreasing trend further out. Thus we do not believe that scattered light affects the measurements in the outer parts of the objects. The wavelength calibration was performed using the average of the two helium–argon arc spectra that bracket the galaxy spectrum.

For each galaxy frame we produced a sky spectrum by averaging an area of the spectrum on the side of the slit opposite to the galaxy nucleus. The averaged sky spectrum was then subtracted from the galaxy spectrum. The quality of the sky subtraction was tested by using regions at various distances from the galaxy centre including galaxy light in the sky spectrum. The systematic effects introduced by sky subtraction errors and galactic light contamination have been discussed in SKP. Similar arguments apply here; we estimate that the maximum allowed systematic error is about 20 km s^{-1} on the last data points (on the order of the errorbars given).

For each galaxy the individual frames were aligned by determining the respective CCD row of each spectrum corresponding to the center of the galaxy. This was defined to be the row containing the highest counts. The aligned spectra were combined by rejecting pixels where the fluxes do not agree within a given limit and by computing the median flux of unrejected pixels. An additional median filtering eliminated the residual cosmic ray hits.

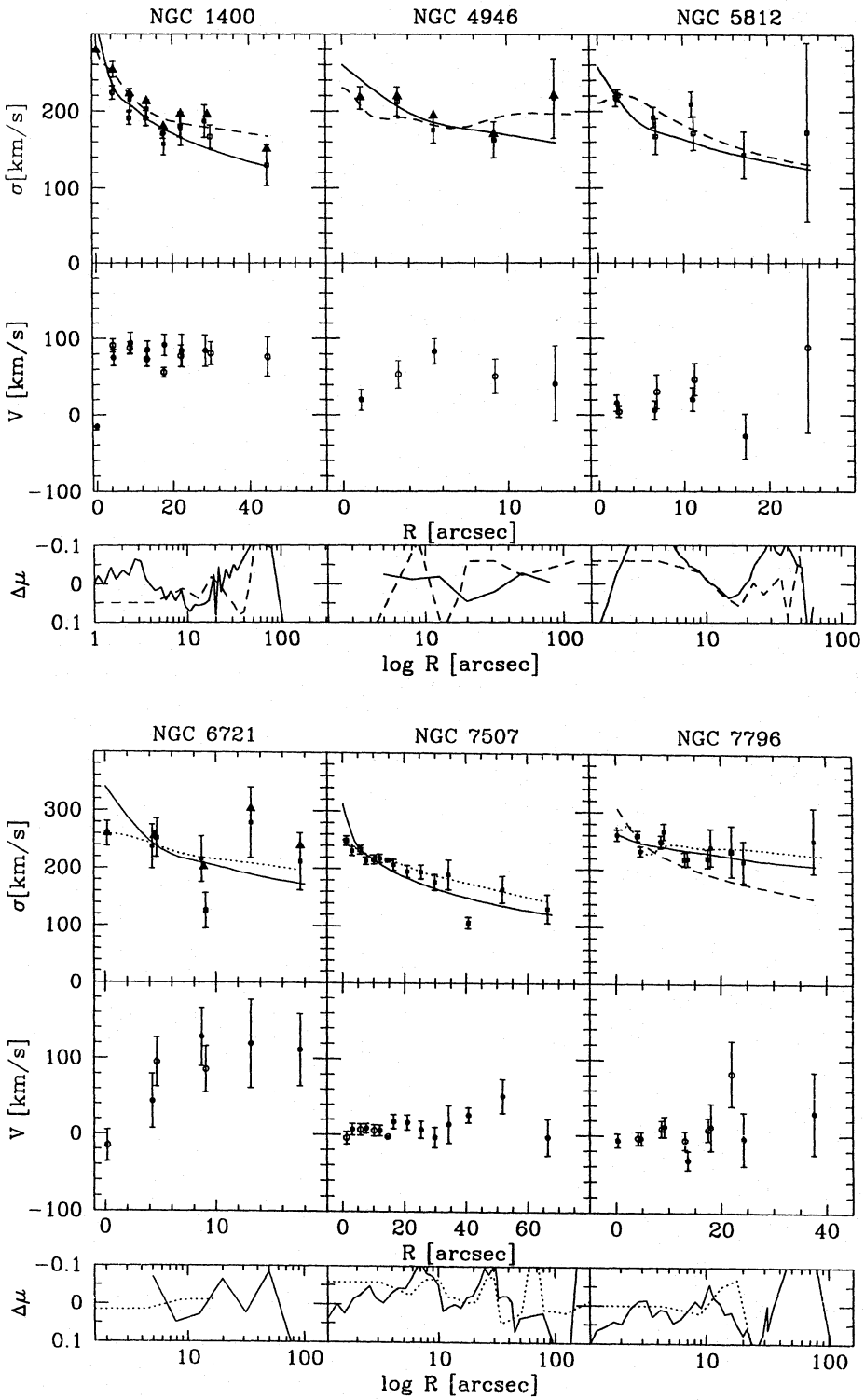

Fig. 1. Top and middle panels: Kinematical profiles along the major axis of NGC 1400, NGC 4946, NGC 5812, NGC 6721, NGC 7507, NGC 7796. Squares (top panels) represent velocity dispersion data, while circles (middle panels) represent radial velocity data. Open and closed symbols refer to the two sides of the galaxies. For NGC 1400, NGC 4946, and NGC 6721 filled triangles give the value of $\mu_2 = (V^2 + \sigma^2)^{1/2}$, averaged on the two sides of the galaxies. The full lines show the velocity dispersion profiles of the best-fit 2C models with no dark halo (best-fit 2C model with dark halo only for NGC 7796; see below), while the short dashed lines are those of the best-fit QP models (see text). Bottom panels: residuals $\Delta\mu = \mu - \mu_{\rm mod}$ between the surface brightness profiles in magnitudes and the projected densities of the best-fit 2C models with no dark halo (full lines, best-fit 2C model with dark halo for NGC 7796) and of the best-fit QP models (short dashed lines). For NGC 7796 the frame with the velocity dispersion profile includes both the best-fit 2C model with dark halo (full line) and the 2C model with no dark halo (long dashed line), showing that dark matter is required in this case

Table 3. Radial velocities, velocity dispersions, and their formal errors (in km s^{-1}) are given as a function of distance to the center (in arcsec)

R	V	δV	σ	$\delta\sigma$
NGC 1400				
−0.10	15.2	0.3	279.1	0.2
−4.55	−75.6	10.5	254.4	10.9
−9.00	−94.4	13.4	215.1	13.9
−13.45	−85.5	11.2	203.1	11.7
−17.90	−91.6	13.5	157.2	14.0
−22.35	−84.1	21	177.2	21.9
−28.53	−84.1	20.2	187.2	21.0
4.35	91.2	8.3	223.9	8.6
8.80	87.9	7.9	191.3	8.2
13.25	73.5	9.3	191.2	9.7
17.70	56.2	6.4	171.4	6.7
22.15	77.5	13.9	180.8	14.5
29.94	81.0	14.7	167.2	15.3
44.73	76.5	25.4	129.9	26.4
NGC 4946				
−1.10	−20.1	13.9	216.9	14.5
−5.55	−83.4	16.2	175.4	16.9
−12.86	−41.2	49.3	216.8	51.4
3.35	53.4	17.9	212.4	18.6
9.22	50.9	22.7	162.8	23.5
NGC 5812				
−2.10	15.9	10.5	217.1	10.9
−6.55	6.5	12.5	192.3	13.1
−11.00	21.1	15.5	209.4	16.2
−17.20	−27.9	29.5	143.4	30.4
2.35	−4.2	7.2	220.8	7.5
6.80	−30.7	22.2	167.4	23.2
11.25	−47.1	21.1	171.6	22.0
24.60	−88.8	112.3	172.9	117.0
NGC 6721				
−4.25	43.6	36.1	237.1	38.0
−8.70	128.1	38.1	215.7	39.8
−13.15	119.2	58.0	279.2	60.8
−17.60	111.6	47.3	211.9	49.5
0.20	15.1	20.8	259.4	21.6
4.65	−95.0	31.9	252.6	33.3
9.10	−85.8	29.9	125.8	30.9

Table 3. (continued)

R	V	δV	σ	$\delta\sigma$
NGC 7507				
−3.15	−7.1	7.6	230.9	7.9
−7.60	−8.4	6.4	213.7	6.7
−12.05	−5.6	7.1	218.2	7.4
−16.50	−17.3	9.4	207.1	9.8
−20.95	−16.3	10.0	195.1	10.4
−25.40	−7.0	11.3	194.7	11.8
−29.85	3.4	13.3	176.8	13.8
−34.30	−13.9	24.9	189.9	25.9
−40.73	−26.3	9.9	106.0	10.1
−51.83	−51.7	22.4	164.8	23.3
−66.47	2.8	23.9	130.6	24.8
1.30	−4.1	8.1	248.6	8.5
5.75	6.8	7.3	233.3	7.6
10.20	5.6	7.5	215.9	7.8
14.65	−2.5	0.8	214.8	0.6
NGC 7796				
−0.27	−6.1	9.1	260.8	9.5
−4.72	−3.4	8.4	232.7	8.7
−9.17	12.1	13.4	267.2	13.9
−13.62	−31.9	12.1	218.9	12.7
−18.07	11.8	31.2	239.5	32.4
−24.27	−3.7	35.1	214.3	36.5
−37.63	30.3	54.6	251.5	56.8
4.18	3.3	8.6	259.7	8.9
8.63	−9.3	10.8	249.3	11.2
13.08	5.8	12.0	218.5	12.5
17.53	−8.3	15.4	220.1	16.0
21.98	−82.3	42.9	232.9	44.5
NGC 7796HR				
−1.46	−13.3	11.6	272.2	12.1
−3.24	−5.9	14.2	268.6	14.8
−5.02	21.4	11.6	249.2	12.1
−7.55	11.6	16.9	201.0	17.5
−13.77	25.4	25.1	219.6	26.2
0.32	−1.3	10.5	273.3	11.0
2.10	10.1	11.5	264.1	11.9
3.88	−7.7	16.7	268.7	17.3
5.66	17.2	13.4	221.8	14.0
8.18	−3.8	10.7	223.8	11.2
19.68	−64.8	16.7	233.7	17.4

3. Kinematics

The spectra of the galaxies were rebinned along the spatial direction in order to obtain a constant S/N ratio (> 15). After removing the continuum, we have endmasked 20% of each spectrum and excluded all frequencies outside the window from wavenumber 5 to 200. Lower wavenumbers are influenced by the continuum subtraction and higher wavenumbers are dominated by noise. Radial velocity V and velocity dispersion σ as a function of radius were derived by means of the Fourier Correlation Quotient (FCQ) technique developed by Bender (1990). The star HR 6884 was used as template for the first observing run and HR 8610 for the second one. No significant differences were noted using other templates. Reliable results were obtained in general out to radial distances of about 20″ from the centre for the first observing run (which was of poorer quality) and of about 40–50″ for the second run.

The kinematical profiles for each galaxy are shown in the upper part of Fig. 1. The central velocity has been subtracted from the radial velocities and the profiles are folded with respect to the centers of the galaxies. The kinematical profiles are symmetric with respect to the center of the galaxies within the

error bars. The results are also presented in tabular form (Table 3).

NGC 1400 has not been observed with long slit spectroscopy before. The kinematical profiles derived from the averaged frame extend out to 45″ from the center, corresponding to 1.2 R_e at a surface brightness of 23.4 mag$_B$ arcsec^{-2}. The galaxy has a flat stellar rotation curve ($V_{max} \approx 90\,km\,s^{-1}$) and a declining velocity dispersion profile.

NGC 4946 shows significant rotation (up to $\approx 80\,km\,s^{-1}$). The velocity dispersion profile and the major axis rotation curve shown in Fig. 1 extend out to $R = 13'' = 0.8\ R_e$, at a surface brightness of 22.0 mag$_B$ arcsec^{-2}.

NGC 5812 shows a declining velocity dispersion profile and little rotation ($\lesssim 40\,km\,s^{-1}$). The profile extends out to $R = 25'' \approx R_e$, at a surface brightness of 20.6 mag$_R$ arcsec^{-2} (or 22.3 in the B band assuming B-R=1.7).

NGC 6721 shows sizable rotational velocity ($\approx 120\,km\,s^{-1}$, see Fig. 1). The kinematical data extend out to $R = 18'' = 0.8R_e$, at a surface brightness of 22.4 mag$_B$ arcsec^{-2}.

NGC 7507 was observed previously by Franx et al. (1989a), who derived kinematical profiles out to $\approx 25''$ from the center, showing that the galaxy has sizable ($50\,km\,s^{-1}$) minor axis rotation. No isophotal twist is present (see Franx et al. 1989b) and the ellipticity is constant. The kinematical profiles derived from our averaged frame extend out to 66″, equal to 2.1 R_e, at a surface brightness of 24.1 mag$_B$ arcsec^{-2}. The galaxy does not show rotation along the major axis and has a declining velocity dispersion profile. In the inner 20″ our data are consistent with the results of Franx et al. (1989a): the mean ratio of measured velocity dispersions (our values to those of Franx et al.) is 1.05 with an rms of 0.03. The error bars inside R_e are always smaller than $15\,km\,s^{-1}$.

NGC 7796 has not been observed previously by means of long slit spectroscopy; no isophotal twisting is present, but isophotes are strongly boxy (Bender, private communication). The velocity dispersion profile is fairly flat out to $R \approx 38''$ (where the surface brightness is 23.3 mag$_B$ arcsec^{-2}) and the rotation velocity is small. Figure 2 shows the results derived from the higher resolution frame. The galaxy has a counterrotating core inside 4″, similar to that observed in several other cases (e.g., see Bender 1988, Franx & Illingworth 1988, Jedrzejewski & Schechter 1988). There is a jump in the velocity dispersion and in the metallicity at 4″, as observed in NGC 4472 and NGC 7626 (Davies et al. 1993) and other galaxies (Bender & Surma 1992). The Mg_2 profile shown in the figure has been derived from the spectra, before continuum subtraction. The error on Mg_2 is estimated to be about 0.02, consistent with the scatter observed between the two sides.

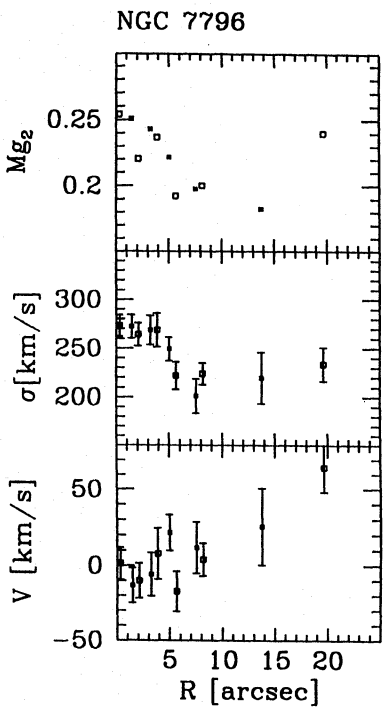

Fig. 2. The counter-rotating core of NGC 7796. Top: Mg_2 line strength profile, Middle: velocity dispersion profile, Bottom: radial velocity profile as a function of the distance from the center. Note the increase in metallicity and in velocity dispersion in the inner 4 arcsec, where the counterrotation takes place. Symbols as in Fig. 1

4. Dynamical models

In the following analysis we have used the CCD photometry in the B band kindly provided by Bender, measured under good seeing conditions, calibrated and extended with the photographic profiles of Lauberts & Valentijn (1989) for NGC 1400, NGC 7507, and NGC 7796. For NGC 5812 we have considered the CCD photometry in the R band by Djorgovski (1985), and for NGC 4946 and NGC 6721 the profiles measured by Lauberts & Valentijn (1989).

As we mentioned in the Introduction, two important factors contribute to determining the shape of the observed velocity dispersion profiles: the possible gradients in the mass-to-light ratio and the structure of the pressure tensor, i.e. the general distribution of stellar orbits. In view of this, here we follow SKP and adopt a two-pronged modelling approach for the interpretation of the stellar dynamical data. Therefore, the surface brightness and the velocity dispersion profiles have been fitted using the procedure and the family of two component models (2C) described by BSS and SBS, and the Quadratic Programming (QP) technique of Dejonghe (1989).

The 2C method considers dynamical models made of two components. The luminous component is characterized by a constant mass–to–light ratio, M_L/L, while the other component represents dark matter, thus allowing for the possibility of a gradient in the cumulative mass–to–light ratio (see Fig. 3 for the best fit model of NGC 7796); as a result, for a given object, the total mass–to–light ratio M/L (see Table 4 and Table 5) can be considerably larger than M_L/L. Note that in these models the dark halo has finite size. Each of the two components is described by an anisotropic distribution function of the Maxwellian type, multiplied by a weight factor of the form $(-E)^{3/2}$, where the specific energy E depends on the poten-

Table 4. Results of the fits

Object	R_e^m ($''$)	R_e^m (kpc)	$\left(\frac{M_L}{L_B}\right)_{2C}$	$\left(\frac{M}{L_B}(R_e^m)\right)_{2C}$	$\left(\frac{M}{L_B}\right)_{2C}$	$\left(\frac{M}{L_B}\right)'$	$\left(\frac{M}{L_B}\right)_{QP}$
NGC 1400	25.3	4.9	3.2	6.0	21.9	4.9	5.1
NGC 4946	20.7	6.5	4.9	9.4	20.5	6.7	6.7
NGC 5812	19.2	3.9	2.9	4.4	9.7	3.4	2.5
NGC 6721	16.3	7.0	4.2	6.9	26.0	5.6	7.8
NGC 7507	38.9	6.6	4.0	6.8	9.8	5.4	5.9
NGC 7796	27.9	8.8	4.7	8.7	31.2	6.7	7.9

Table 5. Trends

Object	$D^{(1)}$ (Mpc)	$M_B^{(1)}$	$SB_e^{(1)}$	$\log_{10} L_x^{(2)}$	$\log_{10} P_5^{(3)}$	$\frac{R_K}{R_e^m}$	R_e^m (kpc)	$\left(\frac{M_L}{L_B}\right)_{2C}$	$\left(\frac{M}{L_B}\right)_{2C}$	$\left(\frac{M}{L_B}\right)_{QP}$	$\left(\frac{M}{L_B}\right)^{(7)}$	$\left(\frac{M}{L_B}\right)$
NGC 1399[4]	28	−21.69	20.68	42.34	22.35	0.88	13.5	8.0	58.0	3.7	6.8	5.1-8.2[8]
NGC 3379[4]	17	−20.72	20.16	<40.36	19.44	1.1	5.1	5.0	11.7	7[13]	3.4	6.3[9]
NGC 4374[4]	27	−22.03	20.81	41.16	23.39	(.49)	17.0	5.3	14.2	5	7.3	8-14[10]
NGC 4472[4,5]	27	−22.84	21.40	42.06	21.93	0.87	16.0	5.0	13.5	12.4	5.9	6.6[9],5-64[10]
NGC 5812[6]	42	−21.22	20.78		< 21.40	1.3	3.9	2.9	9.7	2.5		
NGC 5813[11]	47	−21.97	21.82		20.65	(.57)	35.5	9.1	23.8	8		10-12[11]
NGC 7507[6]	35	−21.57	20.63		< 20.17	1.7	6.6	4.0	9.8	5.9	4.1	3.2[12]
NGC 7626[4]	72	−22.30	21.87	41.55	23.15	0.86	14.3	5.9	33.5	2.5-6.4	6.5	
NGC 7796[6]	65	−21.78	21.41		< 21.78	1.4	8.8	4.7	31.2	7.9		
IC 4296 [5]	75	−23.09	22.07	41.94	24.04	0.93	18	5.6	32.8	16.0	5.7	

References: (1) Faber et al. (1989). (2) Fabbiano, Kim & Trinchieri (1992). (3) Roberts et al. (1991), adjusted to the distances adopted here. (4) SBS. (5) SKP. (6) This paper. (7) van der Marel (1991), from R-band using $L_R/L_B = 1.786$. (8) Bicknell et al. (1989). (9) van der Marel, Binney, and Davies (1990). (10) Katz and Richstone (1985). (11) Efstathiou, Ellis, and Carter (1982). (12) Bacon, Monnet, and Simien (1985). (13) Ciardullo, Jacoby, and Dejonghe (1993).

tial Φ which is generated self-consistently by the *total* density distribution. This choice originates from the physical picture of dissipationless collapse, that envisages that elliptical galaxies have quasi–isotropic pressure inside R_e and a modest excess of radial orbits in the outer regions (see BSS and SBS for full details). The fit, besides the scales M_L/L and R_e^m (the effective radius of the luminous component in the dynamical model), has essentially only three dimensionless free parameters, i.e. the luminous to total mass ratio M_L/M, the parameter that describes how diffuse is the halo (e.g., the ratio of the scalelengths of the two components), and the ratio of central velocity dispersions for the two components.

The QP method complements the first one, in that it assumes a constant mass–to–light ratio and determines a distribution of orbits consistent with the observed velocity dispersion profiles. The QP models assume a representation of the distribution function of stellar orbits as a linear combination of simple terms (typically ten terms are considered in the modeling process), taken to be powers of E and of the total angular momentum of a star. A quadratic programming technique selects a best fit as a set of weights for the simple terms of the polynomial. The program makes sure that the resulting distribution function is positive definite. If this fit is found to be unsatisfactory, in principle QP models can be run with a different choice of potentials, implying variations of M/L with radius, to see whether better fits can be obtained; however, this is not done for the six objects of this paper.

Both methods, 2C and QP, assume spherically symmetric and non-rotating models. In spite of the presence of rotation, we have decided to show the best fit models for NGC 1400, NGC 4946, and NGC 6721, based on the following arguments. Referring to the 2C modeling, we may still argue that, if the galaxy is characterized by quasi–isotropic pressure in the inner regions, then the corrections to mass determinations related to the presence of rotation should be $\approx 0.5V^2/\sigma^2$, as can be shown by discussion of the hydrostatic momentum balance equations (see Michard 1980); thus the M/L ratios determined by fitting the non–rotating models to these three objects might be a reasonable zeroth–order estimate of the true numbers. On the other hand, the presence of significant rotation is an indication that the *physical assumptions* on which the models are based are probably not applicable. Regarding the QP modeling, for the three objects where a significant amount of rotation is present, we have produced models obtained with the device of fitting the second moment $\mu_2 = (V^2 + \sigma^2)^{1/2}$ of the line–of–sight velocity distribution. This procedure goes in the desired direction of including the kinetic energy content associated with V. On the other hand, the presence of rotation indicates that proba-

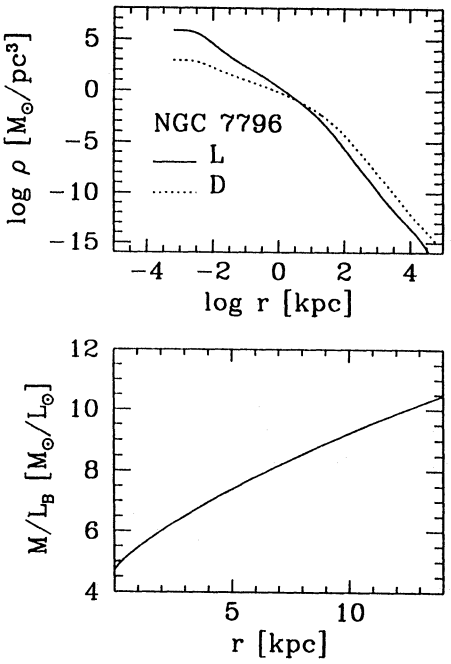

Fig. 3. Luminous-dark matter decomposition derived from the best-fit 2C model for NGC 7796. Volume densities are shown at the top, where the solid line refers to the luminous component and the dotted one to the dark component. The integrated mass-to-light ratio profile is shown at the bottom

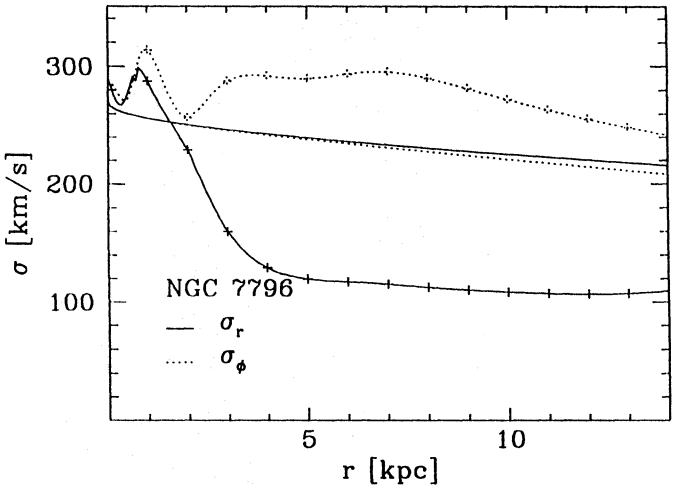

Fig. 4. Unprojected radial (full line) and tangential (dashed line) velocity dispersion profiles derived from the best-fit 2C model, and from the QP model (crosses) for NGC 7796

bly the distribution function (or its even part) cannot be simply reduced to be a function of energy and total angular momentum only. Therefore, the best-fits to NGC 1400, NGC 4946, and NGC 6721, which are shown in Fig. 1 for completeness, are to be taken with caution.

With these qualifications, the results are shown in Fig. 1 and the derived values of the relevant mass-to-light ratios are summarized in Table 4; for uniformity, the last column gives the values of $(M/L_B)_{\rm QP}$ with two digits, even though experience with the QP modeling suggests that they should be given with only one significant digit. Note that the 2C modeling procedure determines a best fit value for the effective radius $R_{\rm e}^m$, which in general differs from the initial, reported value (compare Table 1 with Table 4). In fact, the fitting self–consistent models do not assume an $R^{1/4}$ luminosity profile *a priori* and the choice of the intrinsic effective radius of the model $R_{\rm e}^m$ is made so as to optimize the photometric fit within the radial range of the available surface photometry data.

For all but one of the six galaxies of Fig. 1, good photometric and kinematical fits have been obtained assuming a constant mass-to-light ratio, by both approaches. In order to stress the point, in Fig. 1 the 2C best-fit curves for NGC 1400, 4946, 5812, 6721, and 7507 are replaced by those obtained by strictly one-component models (see Bertin et al. 1988). These fit the data equally well and lead to mass-to-light ratios labeled by $(M/L_B)'$ in Table 4. (The values of $R_{\rm e}^m$ reported in Table 4 are very similar to the values $(R_{\rm e}^m)'$ that are derived from the strictly one–component models.) Therefore, dark halos are not required to explain the decreasing velocity dispersion profiles of NGC 1400, 4946, 5812, 6721, and 7507, even if the best-fit models selected by the 2C method would include a sizable dark component (see Table 4).

NGC 7796 stands out as a different case. In the 2C analysis a satisfactory fit is found only by considering the presence of a sizable second component; Fig. 3 shows the optimal luminous-dark matter decomposition for NGC 7796 suggested by the available spectroscopic and photometric data. On the other hand, the QP modeling shows that the data can be fitted by a constant M/L ratio model only if a large fraction of the orbits are quasi–circular. Figure 4 shows the unprojected radial and tangential velocity dispersion profiles derived for NGC 7796 from the best-fit 2C and from the QP models. (The pressure tensor of the QP model is heavily biased in the tangential direction, since the squares of the velocity dispersions are involved.) The value of M/L found by the QP modeling, $(M/L_B)_{\rm QP} = 7.9$, is on the high side and is similar to the *total* value of M/L_B (due to the contribution of the dark and of the luminous component) of the best–fit 2C model at $1R_{\rm e}^m$, as shown in Fig. 3 and Table 4. Thus, by analogy with the analysis of NGC 4472 and of IC 4296 given in SKP, we conclude that evidence is found for the presence of a dark halo in NGC 7796, although the case is not as strong here, since for this galaxy $(M/L_B)_{\rm QP} < 10$. A plot similar to that of Fig. 4 would show that for the other five objects the pressure tensor of the best fit QP models is smoother and more isotropic; in general, the ratio between radial and tangential velocity dispersion in the main body of these galaxies does not differ from unity by more than 35 per cent.

Finally, we should comment further on the issue of the velocity distribution for the models adopted. While the 2C models are generally characterized by only a moderate bias of orbits in the radial direction in the outer parts (see Fig. 4 for NGC 7796), the QP models tend to have a rather irregular pressure anisotropy profile, with a significantly tangential bias for

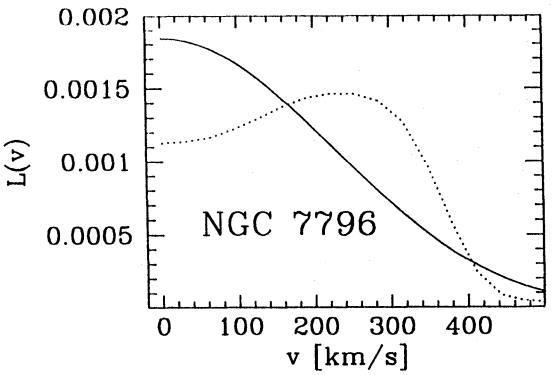

Fig. 5. Line profiles at $R = 35''$ expected for the best–fit QP model (dashed line) and for the best–fit 2C model (full line) of NGC 7796

those cases where the observed velocity dispersion profile is fairly flat (see NGC 7796 in this paper and NGC 4472 or IC 4296 in SKP). Thus, the two approaches lead to different predictions on the line profiles associated with the best-fit models. Figure 5 shows the expected line profile for the best–fit QP and 2C models (the latter profile is kindly provided by O. Gerhard and G. Jeske) of NGC 7796 at $35''$. Methods for extracting these profiles from long slit spectroscopic observations have been the focus of many investigations in recent years (Franx & Illingworth 1988; Bender 1990; Rix & White 1992; Winsall & Freeman 1993; Gerhard 1993; van der Marel & Franx 1993; Cinzano & van der Marel 1993; Kuijken & Merrifield 1993; Saha & Williams 1993). Unfortunately, the quality of our data does not allow us to make a decisive statement on the actual shape of the line profile for any of the six objects of this paper. Still we may mention here that the preliminary finding of gaussian profiles in some galaxies like NGC 4472 for which an attempt has been made (Winsall & Freeman 1993; Bender et al. 1994) does not argue in favor of the extreme 'squarish' QP profile of Fig. 5.

5. Discussion

This paper has presented radially extended kinematical profiles for a small set of objects. If R_K denotes the value of the outermost reliable kinematical datapoint, the values of R_K for the data presented range from $0.8R_e$ (NGC 4946 and NGC 6721) to $2.1R_e$ (for NGC 7507). However, for each galaxy, the value of the effective radius is model dependent. Therefore, for the purpose of discussing the implications of our results on the problem of identifying the global mass distribution, we refer to the value of R_e^m as determined by the dynamical best-fit model. For the six galaxies studied in this article, R_K/R_e^m is in the range from 0.6 (for NGC 4946) to 1.8 (for NGC 1400).

Three of the objects (NGC 1400, NGC 4946, and NGC 6721) appear to be unsuitable for a reliable modeling, not as much because of insufficient quality of the data (which may be a problem for NGC 4946 and for NGC 6721), but especially because of the significant amount of rotation observed (see the case of NGC 1400). To some extent, this might have been suspected from their RC3 classification (see Table 1). The finding of significant rotation is very interesting, because it is a simple direct evidence that argues against intrinsic spherical symmetry, in spite of the fact that the isophotes are fairly round. It would be desirable to have a better appreciation of the frequency of the phenomenon on the basis of a larger sample of objects. On the other hand, for these galaxies our theoretical models, based on distribution functions depending on energy and total angular momentum, are obviously too naive (even though the modeling procedures are able to identify a best-fit model in each case). Thus we limit the following discussion on the presence of dark matter to the three galaxies (NGC 5812, NGC 7507, and NGC 7796; with R_K/R_e^m = 1.3, 1.7, and 1.4, respectively) for which our modeling tools appear to be viable.

In the previous section we have concluded that no evidence for dark matter is found for NGC 5812 and 7507, while NGC 7796 appears to possess a dark halo, much like two other galaxies (NGC 4472 and IC 4296) studied in the same program (SKP). We should try to find a way to interpret such apparently discordant results.

The number of objects at our disposal with radially extended kinematical profiles is very small and they do not define a complete sample in any statistically significant sense. Still it is tempting to look for *possible trends* by combining what we have gathered so far in the most uniform possible way, and by insisting on the quality of the global modeling obtained. Thus we can combine in a single table (see Table 5) the conclusions of this and of two previous papers (SBS and SKP) by adopting the following prescriptions: (i) We retain only objects for which reliable, detailed global modeling is available, (ii) We retain only galaxies for which the kinematical profiles sample a considerable fraction of the galaxy, and this we quantify by requiring that R_K/R_e^m exceeds 0.8. Furthermore, we rescale the results obtained by adopting the distance determination of Faber et al. (1989), so as to have the relative distances internally consistent. Thus the selected galaxies are: NGC 1399, NGC 3379, NGC 7626 from SBS; NGC 4472 (consistent with the results of SBS) and IC 4296 from SKP; NGC 5812, NGC 7507, and NGC 7796 from this paper. In order to further increase the number of objects of the sample, we have also decided to add NGC 4374 (from SBS) and NGC 5813 (data from Efstathiou et al. 1982; 2C and QP modeling performed here), because for these objects the value of R_K/R_e (1.2 and 1.8 respectively) is within the desired range, even if the value of R_K/R_e^m (.49 and .57 respectively) would make us exclude these last two galaxies.

Note that in the list of ten selected objects NGC 1399 is a cD, rather than an elliptical, and NGC 7626 presents kinematical peculiarities, not only in the central regions, but also in the form of appreciable systematic deviations on the large scale from the best–fit model produced. From the point of view of the problem of dark matter, two other objects, NGC 4636 and NGC 7144, would also be interesting, as explained in SBS and SKP. They are not included in Table 5 because they do not satisfy requirements (ii) and (i) respectively.

For comparison, in Table 5 we also list the values of mass–to–light ratios derived by various authors with different meth-

ods. In particular we refer to earlier work based on a generalization of the virial theorem (Bacon et al. 1985), on the Jeans equations (Efstathiou et al. 1982; Bicknell et al. 1989; van der Marel et al. 1990; van der Marel 1991), and on linear programming or maximum entropy techniques (Katz & Richstone 1985).

Surprisingly, we do note some interesting trends in our combined set of galaxies. Firstly, all the objects that have been argued to have a dark halo turn out to have a large value of R_e^m in physical units (larger than 8 kpc), while those for which it has not been possible to argue in favor of a dark halo all have R_e^m smaller than 8 kpc. (In this respect, NGC 7796 is a 'marginal' case.) This might be taken as an indication that dark halos come roughly as objects of the same physical size, so that they would emerge preferentially from the stellar dynamical data only when the luminous galaxy is sufficiently extended. [We should stress that we cannot exclude that those objects for which the available kinematical data do not give convincing evidence for dark matter are actually embedded in massive diffuse halos, as optical and radio studies of spiral galaxies have shown to be the case for disk galaxies (see Introduction)]. Secondly, with the exception of NGC 7796 and 5813, all the objects for which a dark halo has been convincingly invoked turn out to be known bright X-ray sources, while the opposite applies to the case of the remaining galaxies; this is a fact, even though the relevance of X-ray data to the problem of dark matter in ellipticals is still controversial (see Bertin et al. 1993). Finally, if we refer to the M_L/L_B values for the luminous component in the 2C decomposition best-fit model, all of them are in the range 3-9; remarkably, seven out of ten objects have M_L/L_B between 4 and 6. The 2C decomposition seems to identify a stellar component with universal properties, not only in the luminosity profile, but also in the relevant intrinsic population as "summarized" by its mass-to-light ratio. Results obtained from other models tend to go in the same direction. Note instead the large variations in the values of $(M/L_B)_{QP}$ and especially of $(M/L_B)_{2C}$.

Seven of the ten galaxies of Table 5 are known to be radio sources. Table 5 lists the total continuum radio power P_5 at 5 GHz, calculated from the flux listed by Roberts et al. (1991). A strong correlation is found between the total radio power and the total mass M derived from the $\left(\frac{M}{L_B}\right)_{2C}$ values, over almost five decades in radio power. A fit using the ASURV statistical package (LaValley et al. 1992) to take into account the three upper limits yields a probability of less than 0.3% that the correlation is due to chance, and gives $P_5 \propto M^{3.4\pm0.8}$. This sample is of course small, and the results should be interpreted cautiously. Nevertheless, we find that the radio power correlates more strongly with the derived mass than with the observed luminosity. Heckman (1983) also noted a tendency for radio–loud elliptical galaxies to have a higher mass–to–light ratio than radio–quiet ellipticals of the same optical luminosity.

Other correlations (with the absolute luminosity L_B or with the mean surface brightness SB_e) do not show up as sharply in this first exploration, and we do not have a sufficient basis to discuss other potentially interesting issues, such as the behavior of cluster galaxies in comparison to that of field galaxies. The few trends pointed out above have to be taken only as a simple practical way to direct our attention to possibly interesting clues within a very small and biased set of galaxies. We expect that future surveys will allow for a more objective selection of elliptical galaxies.

Acknowledgements. We thank R. Bender for providing his Fourier Correlation Quotient program for the derivation of the kinematical profiles presented here and for making us available the surface photometry used in the fits. We also thank O. Gerhard and G. Jeske for computing one of the line profiles shown in Fig. 5 and R. van der Marel for useful discussions. WWZ acknowledges the support of the Austrian *Fonds zur Förderung der wissenschaftlichen Forschung* (project J0796-PHY).

References

Ashman K.M., 1992, PASP 104, 1109
Bacon R., Monnet G., Simien F., 1985, A&A 152, 315
Bender R., 1988, A&A 202, L5
Bender R., 1990, A&A 229, 441
Bender R., Surma P., 1992, A&A 258, 250
Bender R., Saglia R.P., Gerhard O., 1994, MNRAS 269, 785
Bertin G., Bertola F., Buson L.M., et al., 1989, The Messenger 56, 19
Bertin G., Saglia R.P., Stiavelli M., 1988, ApJ 330, 78
Bertin G., Saglia R.P., Stiavelli M., 1992, ApJ 384, 423 (BSS)
Bertin G., Pignatelli E., Saglia R.P., 1993, A&A 271, 381
Bicknell G.V., Carter D., Killeen N.E.B., Bruce T.E.G., 1989, ApJ 336, 639
Buson L.M., Sadler E.M., Zeilinger W.W., et al., 1993, A&A 280, 409
Ciardullo R., Jacoby G., Dejonghe H., 1993, ApJ 414, 454
Cinzano P., van der Marel R.P., 1993, in: Danziger I.J., Zeilinger W.W., Kjär K. (eds.) Proc. ESO/EIPC Workshop, Structure, Dynamics and Chemical Evolution of Early-Type Galaxies, p. 105
Davies R.L., Sadler E.M., Peletier R.F., 1993, MNRAS 262, 650
Dejonghe H., 1989, ApJ 343, 113
de Vaucouleurs G., 1948, Ann. Ap. 11, 247
de Vaucouleurs G., 1953, MNRAS 113, 134
de Vaucouleurs G., de Vaucouleurs A., Corwin H.G. Jr., et al., 1991, Third Reference Catalogue of Bright Galaxies, Springer, New York
Djorgovski S., 1985, Ph.D. Thesis, Berkeley
Efstathiou G., Ellis R., Carter D., 1982, MNRAS 201, 975
Fabbiano G., Kim D-W., Trinchieri G., 1992, ApJS 80, 531
Faber S.M., Wegner G., Burstein D., et al., 1989, ApJS 69, 763
Franx M., Illingworth G., 1988, ApJ 327, L55
Franx M., Illingworth G., Heckman T., 1989a, AJ 98, 538
Franx M., Illingworth G., Heckman T., 1989b, ApJ 344, 613
Gerhard O., 1993, MNRAS 265, 213
Heckman T.M., 1983, ApJ 273, 505
Illingworth G., 1983, in: Athanassoula E. (ed.) Internal Kinematics and Dynamics of Galaxies, Proc. IAU Symp. 100, Reidel, Dordrecht, p. 257
Jedrzejewski R.J., Schechter P.L., 1988, ApJ 330, L87
Kalnajs A.J., 1983, in: Athanassoula E. (ed.) Internal Kinematics and Dynamics of Galaxies, Proc. IAU Symp. 100, Reidel, Dordrecht, p. 87
Katz N., Richstone D.O., 1985, ApJ 296, 331
Kent S.M., 1986, AJ 91, 1301
Kent S.M., 1990, in: Kron R.G. (ed.) Evolution of the Universe of Galaxies, ASP Conference Series Vol. 10, Brigham Young Univ. Printing Services, p. 109
Kuijken K., Merrifield M.R., 1993, MNRAS 264, 712

Kuijken K.H., Gilmore G., 1989, MNRAS 239, 605
Lauberts A., Valentijn E.A., 1989, The surface photometry catalogue of ESO-Uppsala Galaxies, ESO, Garching
LaValley M.P., Isobe T., Feigelson E.D., 1992, BAAS 24, 839
Merrifield M.R., 1992, AJ 103, 1552
Michard P., 1980, A&A 91, 122
Milgrom M., 1983, ApJ 270, 365
Rix H-W., White S.D.M., 1992, MNRAS 254, 389
Roberts M.S., Hogg D.E., Bregman J.N., Forman W.R., Jones C., 1991, ApJS 75, 751
Saglia R.P., Bertin G., Stiavelli M., 1992, ApJ 384, 433 (SBS)
Saglia R.P., Bertin G., Bertola F., et al., 1993, ApJ 403, 567 (SKP)
Saha P., Williams T.B., 1993, MNRAS (in press)
Sancisi R., van Albada T.S., 1987, in: Observational Cosmology, Proc. IAU Symp. 124, Reidel, Dordrecht, p. 699
Sarazin C.L., 1987, in: de Zeeuw P.T. (ed.) Structure and Dynamics of Elliptical Galaxies, Proc. IAU Symp. 127, Reidel, Dordrecht, p. 179
Tonry J.L., 1983, ApJ 266, 58
van Albada T.S., 1982, MNRAS 201, 939
van Albada T.S., Sancisi R., 1986, Phil. Trans. Roy. Soc. London A 320, 447
van der Marel R., 1991, MNRAS 253, 710
van der Marel R., Binney J., Davies R.L., 1990, MNRAS 245, 582
van der Marel R., Franx M., 1993, ApJ 407, 525
Winsall M.L., Freeman K.C., 1993, A&A 268, 443